Neuron
Article

Essential Role of Presynaptic NMDA Receptors in Activity-Dependent BDNF Secretion and Corticostriatal LTP

Hyungju Park,[1] Andrei Popescu,[1] and Mu-ming Poo[1,2,*]
[1]Division of Neurobiology, Department of Molecular and Cell Biology, Helen Wills Neuroscience Institute, University of California, Berkeley, CA 94720
[2]Institute of Neuroscience, Shanghai Institutes for Biological Sciences, Chinese Academy of Sciences, Shanghai 200031, China
*Correspondence: mpoo@berkeley.edu
http://dx.doi.org/10.1016/j.neuron.2014.10.045

SUMMARY

Activation of N-methyl-D-aspartate subtype of glutamate receptors (NMDARs) in postsynaptic dendrites is required for long-term potentiation (LTP) of many excitatory synapses, but the role of presynaptic axonal NMDARs in synaptic plasticity remains to be clarified. Here we report that axonal NMDARs play an essential role in LTP induction at mouse corticostriatal synapses by triggering activity-induced presynaptic secretion of brain-derived neurotrophic factor (BDNF). Genetic depletion of either BDNF or the NMDAR subunit GluN1 specifically in cortical axons abolished corticostriatal LTP in response to theta burst stimulation (TBS). Furthermore, functional axonal NMDARs were required for TBS-triggered prolonged axonal Ca^{2+} elevation and BDNF secretion, supporting the notion that activation of axonal NMDARs induces BDNF secretion via enhancing Ca^{2+} signals in the presynaptic nerve terminals. These results demonstrate that presynaptic NMDARs are equally important as postsynaptic NMDARs in LTP induction of corticostriatal synapses due to their role in mediating activity-induced presynaptic BDNF secretion.

INTRODUCTION

Postsynaptic activation of N-methyl-D-aspartate subtype of glutamate receptors (NMDARs) at many excitatory synapses is required for activity-dependent induction of long-term potentiation (LTP), a cellular substrate for learning and memory (Bear and Malenka, 1994). However, presynaptic NMDARs are also found in a variety of brain tissues (Brasier and Feldman, 2008; Larsen et al., 2011; McGuinness et al., 2010; Wang and Pickel, 2000) and can regulate glutamate release via elevating presynaptic Ca^{2+} signals (Duguid and Sjöström, 2006; Kunz et al., 2013; McGuinness et al., 2010). Whether presynaptic NMDAR activation also contributes to the LTP induction remains to be thoroughly examined. This possibility was first suggested by the finding in the lateral amygdala where glutamate release from costimulated thalamic inputs could activate presynaptic NMDARs on cortical afferents, leading to heterosynaptic associative LTP at corticoamygdala synapses (Humeau et al., 2003). Here we have directly examined the involvement of presynaptic NMDARs in LTP induction by specific deletion of functional NMDARs from presynaptic axons.

Induction of LTP at some glutamatergic synapses depends on the action of BDNF (Figurov et al., 1996; Korte et al., 1995), a member of neurotrophin family of secreted factors. However, whether BDNF is derived from pre- or postsynaptic neurons and how neural activity controls BDNF secretion at the synapse during LTP induction remain to be clarified (Park and Poo, 2013). Secretion of BDNF from cultured neurons depends on cytoplasmic Ca^{2+} elevation, including contribution of NMDAR-mediated Ca^{2+} influx (Hartmann et al., 2001; Marini et al., 1998; Matsuda et al., 2009), but it is unclear whether axonal NMDARs play a significant role in activity-induced BDNF secretion, and whether axonal BDNF secretion is critical for LTP induction.

In this study, we focused on the role of BDNF secretion in LTP induction at corticostriatal synapses, which may serve for cognitive functions such as instrumental and motor learning (Pennartz et al., 2009). At these synapses, BDNF is likely to be secreted by presynaptic axons, because *Bdnf* mRNA could not be detected in postsynaptic medium spiny neurons (MSNs) in the striatum (Altar et al., 1997; Conner et al., 1997). Given that NMDAR-mediated Ca^{2+} plays a major role in BDNF secretion in cultured neurons, NMDAR activation in cortical axons may directly control presynaptic BDNF secretion at corticostriatal synapses. Thus, we investigated whether LTP at corticostriatal synapses could be induced by theta burst stimulation (TBS), whether LTP induction requires axonal NMDAR activation, and whether axonal NMDARs regulate presynaptic BDNF secretion. By specific deletion of NMDAR subunit GluN1 or BDNF in presynaptic cortical neurons and by direct measurements of activity-induced axonal Ca^{2+} elevation and BDNF secretion, we showed that presynaptic NMDARs are indeed responsible for triggering BDNF secretion via elevating presynaptic Ca^{2+}, leading to LTP at corticostriatal synapses.

RESULTS

Effective Induction of Corticostriatal LTP by TBS

Previous studies demonstrated that reliable LTP at corticostriatal synapses could be obtained when high-frequency stimulation

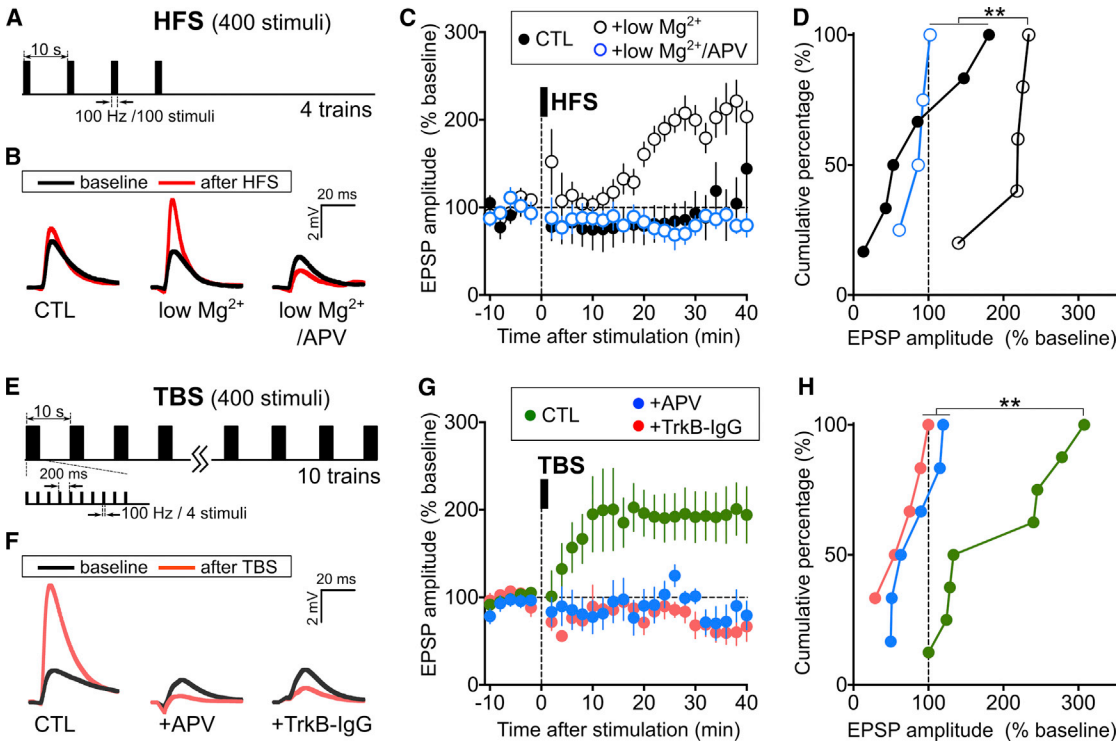

Figure 1. TBS-Induced Corticostriatal LTP Depends on NMDAR Activation and Extracellular BDNF

(A) Schematic diagram depicting the HFS protocol.

(B) Sample traces depict averages of ten EPSPs before (−5–0 min) and after (35–40 min) HFS application from one representative experiment. CTL, 2 mM Mg^{2+} (ACSF, with 100 μM picrotoxin); low Mg^{2+}, low Mg^{2+} ACSF (<200 μM Mg^{2+}); low Mg^{2+}+APV, low Mg^{2+} ACSF with 100 μM APV.

(C) Summary of LTP induction by HFS. The amplitude of EPSPs recorded from MSN cells in the dorsal striatum of parasagittal corticostriatal slices, before and after application of HFS (black bar, 100 Hz train for 1 s, repeated 4 times at 10 s intervals). The EPSP amplitudes from each recording were normalized by the mean amplitude of baseline period prior to HFS. Mean ± SEM (n = 4–6 slices, from at least 2 mice each).

(D) Cumulative percentage plot of mean EPSP amplitudes during 30–40 min after HFS for all experiments described in (C) (percentage of baseline, mean ± SEM; CTL, 87 ± 26; low Mg^{2+}, 207 ± 17; low Mg^{2+}/APV, 86 ± 9; **$p < 0.01$, Kolmogorov-Smirnov test).

(E) Schematic diagram depicting the TBS protocol.

(F) Sample traces depict averages of ten EPSPs before (−5–0 min) and after (35–40 min) TBS application from one representative experiment. CTL, normal ACSF; +APV, normal ACSF with 100 μM APV; +TrkB-IgG, normal ACSF with TrkB-IgG (2 μg/ml).

(G) Summary of LTP induction by TBS. The amplitude of EPSPs recorded and presented as in (C), before and after application of TBS. Mean ± SEM (n = 5–8 slices, from at least 4 mice each).

(H) Cumulative percentage plot of mean EPSP amplitudes during 30–40 min after TBS for all experiments described in (G) (percentage of baseline, mean ± SEM; CTL, 195% ± 29%; +APV, 82% ± 13%; +TrkB-IgG, 63% ± 12%; **$p < 0.01$, Kolmogorov-Smirnov test). See also Figure S1.

(HFS; Figure 1A) of presynaptic axons is applied in a solution containing low-Mg^{2+} (< 200 μM) (Jia et al., 2010; Lovinger, 2010), a condition that favors NMDAR activation via the removal of the Mg^{2+} block (Calabresi et al., 1992). Using whole-cell recording of excitatory postsynaptic potential (EPSPs) in dorsal striatal MSNs in parasagittal brain slices of adult mice, we have examined LTP induction at corticostriatal synapses, with $GABA_A$ receptor-mediated synaptic activity blocked by picrotoxin (100 μM). Consistent with previous findings, HFS of cortical afferents was able to induce corticostriatal LTP (5/5 slices) in low-Mg^{2+} solution, whereas the same HFS in normal Mg^{2+} solution (2 mM) elicited long-term depression (LTD) in the majority of MSNs (4/6), and LTP in minor population of cells (2/6 slices; Figures 1B–1D). The blocking effects of Mg^{2+} and NMDAR antagonist APV (D,L-(2R)-amino-5-phosphonovaleric acid; 100 μM) on LTP (Figures 1B–1D) agree with the previous finding (Jia et al., 2010).

Stimulation of cortical afferents with the TBS reliably induces NMDAR-dependent LTP at these synapses in normal Mg^{2+} solution (Hawes et al., 2013). Consistently, we also found that LTP could be induced from most (7/8) of recorded MSNs by TBS with the same total number of stimuli as that of HFS used above (Figure 1E; see Experimental Procedures). Such TBS-LTP did not depend on dopamine signaling (Figure S1 available online) but required NMDAR activation ($p < 0.01$; Figures 1F–1F). Furthermore, similar to that found for HFS-induced LTP in low-Mg^{2+} condition (Jia et al., 2010), depleting extracellular BDNF by adding soluble BDNF scavenger TrkB-IgG (2 μg/ml) 10–15 min prior to LTP induction prevented synaptic potentiation following TBS ($p < 0.01$; Figures 1F–1F). These results not only show the requirement of NMDAR activation and BDNF secretion in TBS-induced corticostriatal LTP, but also indicate the distinct effectiveness of TBS in NMDAR-dependent LTP induction, as compared to HFS.

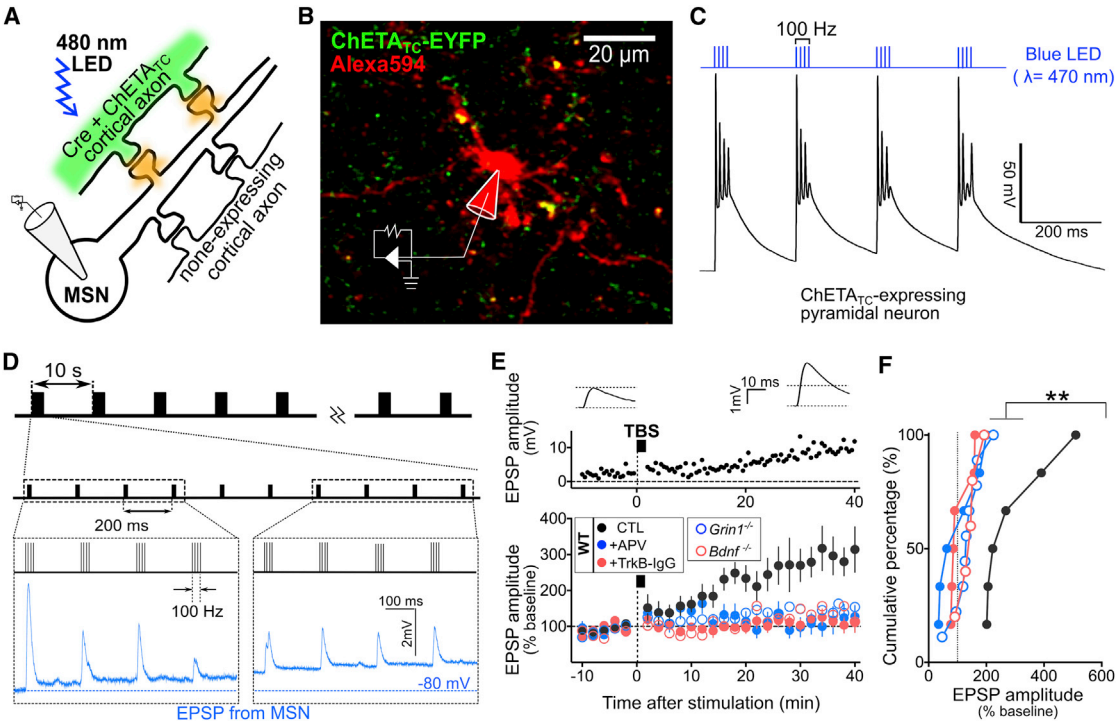

Figure 2. LTP Depends on Functional Axonal NMDARs and BDNF Expression

(A) Schematic diagram depicting the method for optogenetic induction of LTP. Whole-cell recording was made from MSN soma, using striatal slices of wild-type, *Grin1*$^{fl/fl}$, or *Bdnf*$^{fl/fl}$ mice injected with AAVs (AAV-Cre-2a-mCherry and AAV-DIO-ChETA$_{EC}$-EYFP) in M1 area 4 weeks prior to recording. Axons expressing ChETA$_{EC}$-EYFP and Cre (green) were selectively activated by light pulses (0.2–1 ms; λ = 480 nm).

(B) Representative confocal image of a striatal slice showing cortical axons expressing ChETA$_{TC}$ (green) and the MSN (and its dendrites) that was loaded with Alexa 594 dye (red) via the whole-cell recording pipette.

(C) Schematic diagram of the TBS pattern of the light stimuli for LTP induction, together with an example of light-evoked composite EPSP responses in a striatal MSN in response to successive burst stimuli.

(D) Top: representative traces (average of ten EPSPs) showing light-evoked EPSP responses during the baseline period (−5–0 min; left) or 35–40 min after light pulses with the TBS pattern (right). Bottom: data from one representative experiment showing increased EPSP responses after optogenetic stimulation. Black bar, light pulses with the TBS pattern.

(E) Summary of all optogenetic LTP experiments. Mean EPSP amplitudes evoked by test light pulses (at 0.5 Hz), shown as normalized mean EPSP amplitude before and after optogenetic TBS (marked by the bar). Wild-type mice ("WT"): in the absence ("CTL," 291% ± 44% of the baseline at 30–40 min) or the presence of either "APV" (100 μM, 106% ± 29%) or "TrkB-IgG" (2 μg/ml, 109% ± 160%). "*Bdnf* $^{-/-}$" (142% ± 17%) and "*Grin1* $^{-/-}$" (135% ± 17%): data from mice with the *Bdnf* and *Grin1* gene deleted by expressing Cre in *Bdnf*$^{fl/fl}$ and *Grin1*$^{fl/fl}$ mice, respectively. Mean ± SEM. (n = 5–9 slices, at least 4 mice each).

(F) Cumulative percentage plot of mean amplitudes of EPSPs during 30–40 min after optogenetic TBS from corticostriatal slices for data shown in (E) (**$p < 0.01$, Kolmogorov-Smirnov test). See also Figure S2.

Requirement of Axonal NMDAR Activation for TBS-Induced LTP

We next explored the mechanisms responsible for TBS-induced corticostriatal LTP. Previous studies of hippocampal CA3-CA1 synapses showed that TBS in physiological Mg^{2+}-containing solution could induce a form of LTP that involves presynaptic facilitation of transmitter release and requires the expression of presynaptic BDNF (Zakharenko et al., 2001, 2003). At corticostriatal synapses, TBS-induced LTP also depended on NMDAR activation (Figures 1G and 1H), but whether presynaptic NMDARs are involved is unknown. We thus directly examined this issue by deleting the crucial NMDAR subunit GluN1 (Tsien et al., 1996) from presynaptic cortical neurons with a conditional gene-deletion method. To achieve this goal, we coinjected an adeno-associated virus (AAV) vector coding for Cre and mCherry (AAV-CMV-Cre-2a-mCherry) together with another AAV vector containing Cre-dependent gene expression cassette coding for a high-efficiency channelrhodopsin-2 (ChR2) variant for faster neuronal stimulation (ChETA$_{TC}$; AAV-DIO[double floxed inversed open reading frame]-hChR2 (E123T/T159C)-EYFP) (Berndt et al., 2011) into the primary motor cortex (M1) of either wild-type (WT) mice or knockin mice (*Grin1*$^{fl/fl}$), in which the GluN1 gene (*Grin1*) is flanked by two *loxP* sites (Tsien et al., 1996). These mice were used for slice recording 4 weeks after viral injection. The expression of the two AAV vectors should result in Cre-dependent *Grin1*-deletion together with ChETA$_{TC}$-EYFP expression in the same cortical neurons in *Grin1*$^{fl/fl}$ mice (Figure 2A and Figure S2A), due to the requirement of Cre-mediated recombination for ChETA$_{TC}$- EYFP expression. Cre-dependent depletion of GluN1 expression was confirmed by the absence of immunostaining of GluN1 proteins in Cre-expressing neurons in M1 and at M1-derived axons in the dorsal striatum of AAV-injected

Grin1$^{fl/fl}$ mice (Figure S2A) and the lack of NMDA-induced inward current at Cre-expressing cortical neurons in M1 of AAV-injected *Grin1*$^{fl/fl}$ mice, in comparison to control neurons (Figure S2B).

We then examined whether optogenetic light stimulation could depolarize ChETA$_{TC}$-expressing M1 neurons with the burst pattern and evoke synaptic responses in striatal MSNs, using WT mice injected with the above-mentioned two AAV vectors. In these mice, ChETA$_{TC}$ was expressed in M1 axons without *Grin1* deletion (Figure S2A). Whole-cell recording from the soma of M1 pyramidal neurons expressing ChETA$_{TC}$ in coronal slices (Figure S2D) showed reliable spiking in response to brief light pulses (0.2–1.0 ms; $\lambda = 480$ nm) with only occasional failures during 100 Hz burst stimulation (Figure S2E). In addition, light stimuli with the TBS pattern induced composite EPSPs similar with those induced by the TBS-patterned electrical stimulation, but with a more rapid time to peak (Figure 2C; Figures S2F–S2I).

Recording from MSNs of the dorsolateral striatum showed that "test" stimuli (single light pulses at a low frequency; 0.03 Hz) reliably evoked EPSPs with a constant amplitude (Figure 2D). Moreover, these TBS-patterned light stimuli also produced a persistent increase in the amplitude of EPSPs evoked by test light stimuli from all of recorded slices (6 of 6 slices; Figure 2E). Furthermore, optogenetic TBS-induced LTP at these synapses was largely absent when NMDARs were blocked by APV treatment or extracellular BDNF was chelated by TrkB-IgG, a soluble ligand that binds BDNF ($p < 0.01$; Figures 2E and 2F). Thus, optogenetic LTP induced by light stimuli with the TBS pattern is comparable to electrically induced LTP. Further analyses were performed to examine whether pre- or postsynaptic properties were altered after LTP induction. When changes in the coefficient of variation (CV) were analyzed by plotting $1/CV^2$ against TBS-induced changes in the mean EPSP amplitude (normalized by the basal EPSP amplitudes) (Faber and Korn, 1991), we found that the expression of LTP involved an increase in the probability of presynaptic release (Figure S2J). Consistently, the paired-pulse ratio (PPR; interstimulus interval [ISI] = 50 ms) of EPSP amplitude at 30 min after TBS was significantly reduced as compared to that found prior to TBS ($p < 0.05$; Figure S2K). In addition, we found TBS-induced postsynaptic modification, as indicated by a significant decrease in the ratio of NMDAR- and AMPAR-mediated evoked postsynaptic excitatory currents (EPSCs; NMDA/AMPA ratio) following optogenetic TBS ($p < 0.05$; Figure S2L). Thus, TBS-induced LTP is accompanied by both pre- and postsynaptic changes.

We next examined optogenetic LTP induction in *Grin1*$^{fl/fl}$ mice with Cre-dependent deletion of GluN1 in M1 axons. In contrast to that found in control WT mice, the same optogenetic TBS resulted in significantly diminished LTP in striatal slices from *Grin1*$^{fl/fl}$ mice ($p < 0.01$; Figures 2E and 2F), indicating that functional axonal NMDARs are required for corticostiatal LTP. Dendritic NMDARs of cortical neurons are unlikely to be involved because the coronal sectioning of these striatal slices had severed the axons from their cell bodies in M1. Analyses of basal EPSP responses and composite EPSPs showed that TBS-patterned light stimuli were not affected by inhibiting NMDARs or depleting GluN1 expression in cortical axons (Figures S2N–S2Q), indicating that the lack of LTP was not due to altered NMDAR-mediated actions on synaptic transmission. Finally, we found that postsynaptic NMDARs are also required for TBS-induced LTP, because optogenetic TBS failed to induce LTP when postsynaptic NMDARs were blocked by the NMDAR antagonist MK-801 (1 mM; see Humeau et al., 2003) that was dialyzed into the recorded MSN via the recording pipette (Figure S2M).

Requirement of Axonal BDNF in TBS-Induced LTP

The importance of axonal BDNF in TBS-induced LTP was further examined by selectively eliminating BDNF expression with *Cre-loxP* deletion of *Bdnf* gene in M1 cortical axons using the same strategy of AAV infection (see Experimental Procedures; Figures S2R and S2S). We found that deletion of BDNF expression at cortical axons caused reduced basal synaptic transmission and significantly lower composite EPSP responses during TBS (Figures S2N–S2Q), indicating a presynaptic impairment caused by reduced BDNF expression. These results are similar to those found at Schaffer collateral-CA1 synapses of *Bdnf* knockout mice (Patterson et al., 1996; Pozzo-Miller et al., 1999). Furthermore, we found that optogenetic TBS failed to induce significant LTP when *Bdnf*-deficient cortical axons were stimulated in striatal slices from *Bdnf*$^{fl/fl}$ mice ($p < 0.01$; Figures 2E and 2F). Thus, induction of corticostrital LTP by TBS requires both NMDARs and BDNF in the presynaptic axons. The reduced basal synaptic transmission in slices with presynaptic BDNF deletion may result in a suboptimal activation of postsynaptic NMDARs during TBS, accounting in part for the failure of LTP induction.

The notion that secreted BDNF could induce synaptic potentiation is further supported by the finding that the basal synaptic transmission at corticostriatal synapses was elevated by treatment of the brain slices with exogenous BDNF (200 ng/ml), but the APV treatment prevented such BDNF-induced synaptic potentiation (Figures S2T and S2U). This NMDAR dependency and the similarities in the time course and magnitude of potentiation between BDNF- and optogenetic TBS-induced potentiation suggest both forms are mediated by similar mechanisms.

Axonal NMDARs Elevate Activity-Induced Presynaptic Ca^{2+}

Since BDNF secretion is known to be Ca^{2+} dependent (Lessmann and Brigadski, 2009), enhanced Ca^{2+} elevation due to activation of axonal NMDARs may account for the requirement of functional axonal NMDARs for LTP induction. We examined this possibility by direct measurements of Ca^{2+} changes in presynaptic cortical axons, using Ca^{2+} sensor GCaMP5 (Akerboom et al., 2012) specifically expressed in M1 cortical axons. An AAV vector containing Cre-dependent GCaMP5 construct was injected into M1 of *Emx1-Cre* mice, and corticostriatal slices of injected mice were examined after 2 weeks. We found that electrical stimulation of M1 axons with the TBS pattern induced a prolonged elevation of GCaMP5 fluorescence in cortical axons in the dorsal striatum (Figure 3A) that decayed to the baseline by ~400 s after TBS (Figure 3A). Furthermore, we found that the initial Ca^{2+} elevation (30–90 s after TBS) was mostly inhibited by the pretreatment with $CdCl_2$ (100 μM) or Ca^{2+}-free solution (2 mM EGTA-containing ACSF with no Ca^{2+}), indicating the

requirement of extracellular Ca^{2+} influx through Ca^{2+}-permeable channels ($p < 0.0001$, CTL versus Ca^{2+}-free or $CdCl_2$; Figures 3A and 3B). On the other hand, the sustained Ca^{2+} elevation after the stimulation period (100–300 s after TBS) was largely dependent on Ca^{2+} release from internal stores, because prolonged axonal Ca^{2+} level was not observed when intracellular Ca^{2+} store was depleted by the pretreatment with cyclopiazonic acid (CPA; 30 μM) ($p < 0.01$, CTL versus CPA; Figures 3A and 3B). Moreover, TBS-induced long-lasting Ca^{2+} elevation was also largely abolished by the presence of APV ($p < 0.01$, CTL versus APV; Figures 3A and 3B), consistent with the involvement of NMDARs in mediating axonal Ca^{2+} accumulation that triggers Ca^{2+} release from internal stores. Finally, this prolonged axonal Ca^{2+} elevation was not due to deleterious Ca^{2+} responses caused by electrical stimulation, since optogenetic TBS of M1 axons of *Emx1-Cre* mice expressing both GCaMP5 and ChETA$_{TC}$-mCherry showed the robust TBS-induced prolonged Ca^{2+} elevation (up to ~400 s), which was eliminated by pretreatment with APV (Figure S3).

Since HFS-induced LTP in low-Mg^{2+} condition also requires extracellular BDNF (Jia et al., 2010), which is likely to be secreted from cortical axon terminals in response to elevated Ca^{2+}, we further examined whether HFS is also capable of evoking NMDAR-dependent axonal Ca^{2+} elevation. We found that HFS induced very small axonal Ca^{2+} increase in the normal Mg^{2+} solution but a robust axonal Ca^{2+} elevation in the low-Mg^{2+} solution that was largely abolished by APV (Figures 3C and 3D). These results support the notion that the low-Mg^{2+} condition facilitates the activation of presynaptic NMDARs induced by HFS-evoked glutamate release, with the consequent Ca^{2+} elevation that is required for triggering BDNF secretion and LTP (see sections below).

To directly test the role of axonal NMDARs in TBS-induced Ca^{2+} elevation, we deleted *Grin1* selectively in M1 cortical neurons by coinjecting AAV containing synapsin promoter-driven GCaMP5 (AAV-hSyn-GCaMP5) with AAV-CMV-Cre-2a-mCherry into M1 of *Grin1*$^{fl/fl}$ mice (Figure 3E). This allowed us to compare GCaMP5 signals from axons with functional NMDARs (expressing only GCaMP5; "*Grin1*-CTL") and axons with GluN1 deletion (coexpressing GCaMP5 and Cre; "*Grin1*$^{-/-}$") in the same parasagittal corticostriatal slices (Figure 3E). We found a sustained GCaMP5 signals in "*Grin1*-CTL" axons in the dorsal striatum by electrical TBS, and this Ca^{2+} elevation was reversibly abolished by APV (Figures 3F and 3G), consistent with the involvement of NMDARs in TBS-induced Ca^{2+} accumulation. By contrast, the same TBS failed to induce the sustained Ca^{2+} elevation in GluN1-deleted axons in the same slices ($p < 0.01$; Figure 3H). Thus, activation of axonal NMDARs is indeed required for TBS-induced axonal Ca^{2+} accumulation.

BDNF Secretion Requires NMDAR Activation

Using immunostaining of MYC-tagged BDNF proteins in *Bdnf-myc* knockin mice (Dieni et al., 2012), we found that most of endogenous BDNF-MYC proteins in the dorsal striatum were localized to dense core vesicles in cortical axons, as shown by their colocalization with the dense core vesicle marker chromogranin B or with the dye tracer preloaded into M1 neurons (Figure S4), but no significant expression of endogenous BDNF-MYC in striatal cells or dopaminergic fibers (Figure S4). This is consistent with the cortical origin of striatal BDNF (Altar et al., 1997). Given that TBS could effectively induce the prolonged Ca^{2+} elevation in cortical axons (Figure 3), axonal BDNF secretion is thus likely to be triggered by TBS via NMDAR-dependent Ca^{2+} signaling.

To directly observe NMDA-dependent BDNF secretion from cortical axons in the striatum, we expressed BDNF tagged with a fluorescence protein. This is because the concentration of endogenous BDNF is extremely low (~150 ng/g tissue weight) in the adult brain (Matsumoto et al., 2008) and there is no reliable method for detecting such a low concentration within the living tissue. A *Bdnf* construct was fused with the cDNA of a pH-sensitive fluorescent protein (superecliptic pHluorin; BDNF-pH) (Matsuda et al., 2009), which is known to undergo the same intracellular processing and exhibits similar biological activity as the native BDNF (Matsuda et al., 2009; see Discussion). To restrict the expression of BDNF-pH in cortical pyramidal neurons, we injected an AAV vector containing double-floxed inversed BDNF-pH codon into the M1 of *CaMKIIa-Cre* or *Emx1-Cre* mice (Figure 4A). At 2 weeks after virus injection, we observed high-level BDNF-pH expression in corticostriatal axons innervating the dorsal striatum (Figure 4A), with axonal BDNF-pH puncta largely localized to areas marked with the presynaptic marker synaptophysin and juxtaposed to the postsynaptic marker PSD-95 (Figures 4B and 4C). Using time-lapsed two-photon microscopy of parasagittal corticostriatal slices, activity-induced BDNF secretion was monitored by changes in the fluorescence intensity of BDNF-pH puncta, which represent individual or clustered BDNF-containing granules (Matsuda et al., 2009).

Previous studies using BDNF-pH have shown that BDNF-containing granules in axons may undergo activity-dependent exocytic fusion either with or without secretion of the granular content (Matsuda et al., 2009). This is usually indicated by an initial fluorescence increase (opening of fusion pore and exposure of BDNF-pH to higher pH environment), followed by gradual fluorescence reduction back to the basal level ("fusion without secretion") or below the basal level ("fusion with secretion") (Matsuda et al., 2009). Upon TBS of cortical axons, we found that most fluorescent puncta exhibited fusion with secretion, with an overall reduction of BDNF-pH fluorescence below the basal level (Figures 4D–4F). Such fluorescence reduction was largely diminished when TBS was applied in the presence of APV (100 μM; Figures 4G; $p < 0.01$) but not affected by dopamine signaling (Figure S4H), consistent with results of TBS-LTP. On the other hand, HFS induced robust BDNF-pH fluorescence reduction in the low-Mg^{2+} condition, but the fluorescence decrease was switched to the increase by adding APV or normal Mg^{2+} to the recording solution (Figures 4F and 4G; $p < 0.001$, low Mg^{2+} versus normal Mg^{2+} or low Mg^{2+}/APV). These results suggest that NMDAR-mediated Ca^{2+} elevation is crucial for axonal BDNF secretion, although the fusion without secretion of BDNF-containing vesicles may occur via NMDAR-independent mechanisms. Finally, we found that TBS failed to trigger axonal BDNF secretion and LTP induction when internal Ca^{2+} stores were depleted by pretreatment with CPA (Figures S4H–S4K),

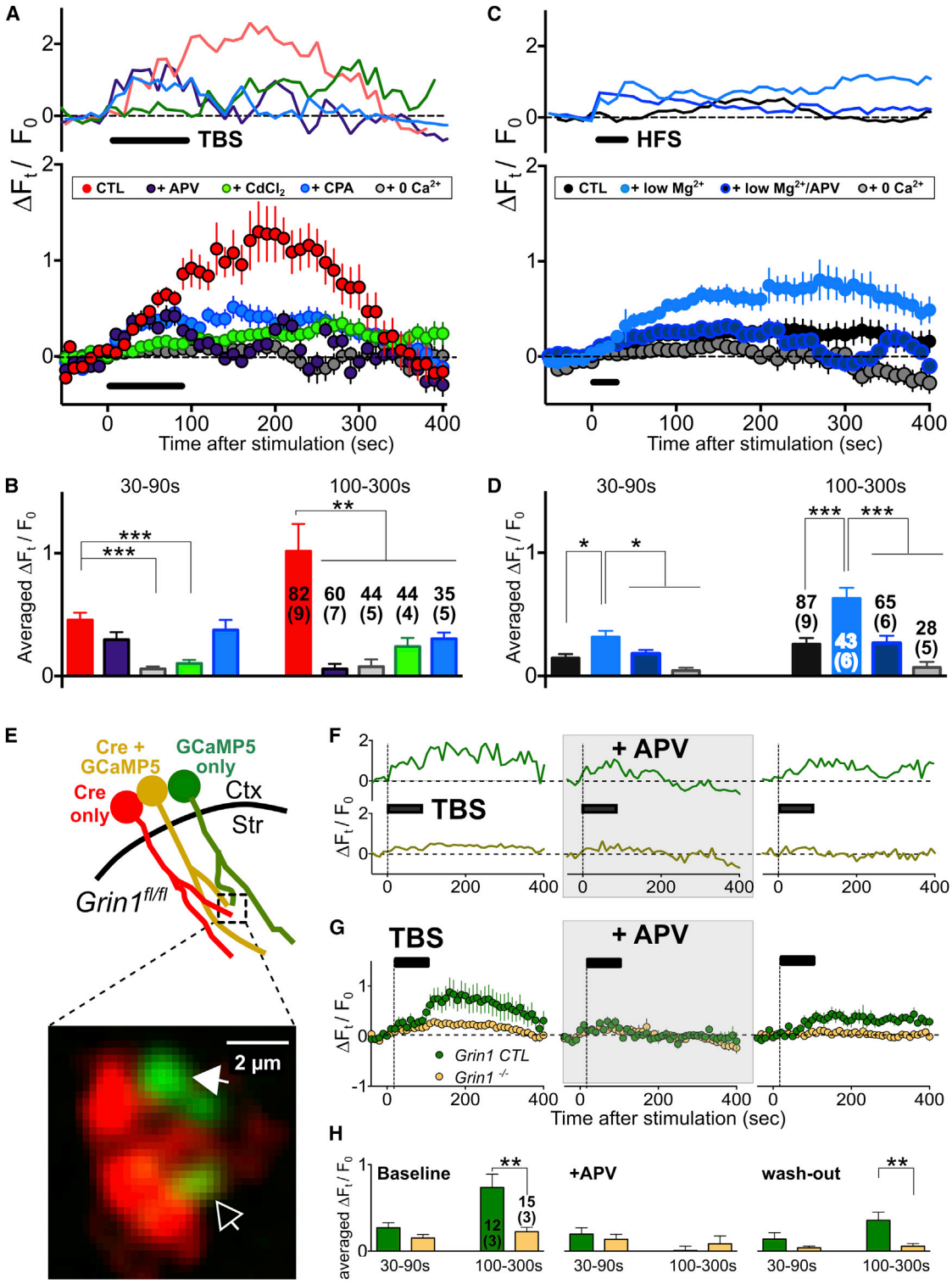

Figure 3. TBS-Induced Ca^{2+} Elevation in Cortical Axons Depends on Axonal NMDARs

(A) Measurements of GCaMP5 fluorescence signals from cortical axon terminals in the dorsal striatum. Top traces: sample recordings of TBS-induced GCaMP5 fluorescence from a representative experiment. Different experimental conditions are coded by colors (same as the graph below). The graph depicts the results from all experiments on TBS-induced fractional changes in GCaMP5 fluorescence with time ($\Delta F_t/F_0$). Mean ± SEM (n = 44–82 at least from 4 slices). CTL (control),

(legend continued on next page)

confirming the importance of Ca^{2+} release from internal stores for TBS-induced BDNF secretion and LTP.

Axonal BDNF Secretion Requires Axonal NMDARs

Our immunostaining analysis showed that endogenous BDNF-MYC proteins were stored in cortical axons that express functional NMDARs (Figure S5). The finding that the conditions for axonal BDNF release were the same as those for axonal NMDAR-dependent Ca^{2+} elevation (Figure 3) suggests that axonal BDNF secretion is directly controlled by presynaptic NMDARs. To test this idea, we coinjected AAV-hSyn-BDNF-pH and AAV-Cre-2a-mCherry in M1 of *Grin1*$^{fl/fl}$ mice, in order to achieve both Cre-loxP-mediated GluN1 deletion and BDNF-pH expression in M1 cortical axons (Figure 5A). We found that the fluorescence intensity of axonal BDNF-pH puncta was reduced following TBS in axons containing normal NMDARs (expressing only BDNF-pH; "*Grin1*-CTL"), but not in axons with *Grin1* deletion (coexpressing BDNF-pH and Cre; "*Grin1*$^{-/-}$") in the same parasagittal corticostriatal slice (Figures 5B and 5C), indicating that BDNF secretion depends on functional NMDARs. As summarized in Figures 5D and 5E, average fractional changes in the puncta fluorescence ($\Delta F_t/F_0$) during 100–200 s after TBS were significantly different between the two groups ($p < 0.01$). In addition, TBS-induced BDNF-pH fluorescence reduction was normal in Cre-expressing axons of AAV-injected WT mice, indicating that the absence of fluorescence reduction in *Grin1*$^{-/-}$ axons was not due to nonspecific effects of Cre and mCherry expression (Figures 5D and 5E). Together with the findings on the dependence of LTP on both axonal NMDAR activation and BDNF expression (Figure 2), these results support the notion that axonal NMDARs play an essential role in TBS-induced LTP at corticostriatal synapses by controlling BDNF secretion from cortical axons.

DISCUSSION

In this study, we provided direct evidence that presynaptic NMDARs play an essential role in activity-dependent presynaptic BDNF secretion and LTP induction at corticostriatal synapses. Similar to their action at postsynaptic sites, activated presynaptic NMDARs enhance Ca^{2+} level in the axon terminal, facilitating exocytosis of synaptic vesicles (Duguid and Sjöström, 2006; Kunz et al., 2013; McGuinness et al., 2010) as well as BDNF-containing secretory granules (Figure 6). The involvement of presynaptic NMDAR-mediated prolonged Ca^{2+} elevation in BDNF secretion is in line with the requirement of global Ca^{2+} accumulation for the exocytosis of secretory granules (Pang and Südhof, 2010; Peng and Zucker, 1993). Since the main source of secreted BDNF at corticostriatal synapses is presynaptic, axonal NMDAR activation is of particular importance to BDNF-dependent LTP at these synapses. At other synapses where BDNF could be secreted from postsynaptic dendrites, whether presynaptic NMDAR activation also contributes to LTP remains to be investigated.

LTP Induced by Optogenetic versus Electrical Stimulation

We have used an optogenetic method to induce LTP at corticostriatal synapses by optical activation of high-efficiency ChR2 ($ChETA_{TC}$)-expressing axons with TBS-patterned light illumination. Our data showed that brief light pulses at high frequencies are capable of triggering fast and efficient neuronal excitation with occasional failures in the later spikes within the 100 Hz

ACSF (with 2 mM Mg^{2+} and 100 μM picrotoxin); +APV, ACSF with 100 μM APV; $CdCl_2$, ACSF with 100 μM $CdCl_2$; +CPA, normal ACSF with 30 μM CPA; 0 Ca^{2+}, ACSF with no added Ca^{2+} and 2 mM EGTA.

(B) Summary of average $\Delta F_t/F_0$ (±SEM) during 30–90 s and 100–300 s after TBS application. Colors on the bar are same as in (A). Numbers of puncta and slices (with bracket) are shown with the bars (**$p < 0.01$; ***$p < 0.001$; one-way ANOVA with post hoc test). Averaged $\Delta F_t/F_0$ during 30–90 s: CTL, 0.45 ± 0.06; APV, 0.30 ± 0.06; $CdCl_2$, 0.10 ± 0.03; CPA, 0.30 ± 0.05; 0 Ca^{2+}, 0.06 ± 0.02. Averaged $\Delta F_t/F_0$ during 100–300 s: CTL, 1.02 ± 0.22; APV, −0.05 ± 0.04; $CdCl_2$, 0.24 ± 0.07; CPA, 0.37 ± 0.08; 0 Ca^{2+}, 0.08 ± 0.06.

(C) Measurements of GCaMP5 fluorescence signals from cortical axon terminals in the dorsal striatum. Top traces: sample recordings of HFS-induced GCaMP5 fluorescence from a representative experiment. Different experimental conditions are coded by colors (same as the graph below). The graph depicts results from all experiments on HFS-induced fractional changes in GCaMP5 fluorescence with time ($\Delta F_t/F_0$). Mean ± SEM (n = 28–87 at least from 5 slices). CTL, ACSF (with 100 μM picrotoxin, 2 mM Mg^{2+}); low Mg^{2+}, low-Mg^{2+} ACSF (<200 μM Mg^{2+}); low Mg^{2+}/+APV, low-Mg^{2+} ACSF with 100 μM APV; 0 Ca^{2+}, ACSF with no added Ca^{2+} and 2 mM EGTA.

(D) Summary of the average $\Delta F_t/F_0$ (±SEM) during 30–90 s and 100–300 s after HFS application. Color codes are same as in (C). Numbers of puncta and slices (with bracket) are shown with the bars (*$p < 0.05$; ***$p < 0.01$; one-way ANOVA with post hoc test). For 30–90 s: CTL, 0.14 ± 0.03; low-Mg^{2+}, 0.31 ± 0.04; low-Mg^{2+}/+APV, 0.18 ± 0.03; 0 Ca^{2+}, 0.04 ± 0.02. For 100–300 s: CTL, 0.25 ± 0.05; low-Mg^{2+}, 0.63 ± 0.09; low-Mg^{2+}/+APV, 0.26 ± 0.06; 0 Ca^{2+}, 0.07 ± 0.05.

(E) Schematic diagram showing striatal slices of *Grin1*$^{fl/fl}$ mice expressing Cre-2a-mCherry and GCaMP5 in M1-derived axons. Red, Cre (mCherry) only; green, GCaMP5 only; yellow, Cre + GCaMP5. The fluorescence image below at a higher resolution shows a representative dorsal striatal area containing these three types of axons. Empty arrowhead: axon expressing Cre + GCaMP5. Filled arrowhead: axon expressing only GCaMP5.

(F) Representative recording traces of GCaMP5 fluorescence changes with time ($\Delta F_t/F_0$) recorded from the GCaMP5-only axon (green), and axon coexpressing GCaMP5 and Cre (yellow) during three episodes of TBS (bar), prior to and after APV was added, as well as after APV was washed out. No GCaMP5 signal was detected from axons expressing only Cre.

(G) Summary of all data (mean ± SEM; n = 12–15) recorded in a similar manner as shown in (F), for axons expressing only GCaMP5 ("*Grin1*-CTL") and axons expressing both GCaMP5 and Cre ("*Grin1*$^{-/-}$") in three striatal slices.

(H) Summary of average $\Delta F_t/F_0$ (±SEM) during 30–90 s and 100–300 s after TBS application. Color codes are same as in (F) and (G). Numbers of puncta and slices (with bracket) from two mice are shown with the bars (**$p < 0.01$; unpaired t test). In the control condition (baseline), averaged $\Delta F_t/F_0$ during 30–90 s: *Grin1* CTL = 0.27 ± 0.06; *Grin1*$^{-/-}$ = 0.15 ± 0.04, averaged $\Delta F_t/F_0$ during 100–300 s: *Grin1* CTL = 0.74 ± 0.15; *Grin1*$^{-/-}$ = 0.22 ± 0.05. In the presence of APV (+APV), averaged $\Delta F_t/F_0$ during 30–90 s: *Grin1* CTL = 0.20 ± 0.07; *Grin1*$^{-/-}$ = 0.14 ± 0.06, averaged $\Delta F_t/F_0$ during 100–300 s: *Grin1* CTL = 0.01 ± 0.05; *Grin1*$^{-/-}$ = 0.09 ± 0.09. After APV was washed out (wash-out), averaged $\Delta F_t/F_0$ during 30–90 s: *Grin1* CTL = 0.14 ± 0.07; *Grin1*$^{-/-}$ = 0.04 ± 0.02, averaged $\Delta F_t/F_0$ during 100–300 s: *Grin1* CTL = 0.35 ± 0.09; *Grin1*$^{-/-}$ = 0.05 ± 0.03. See also Figure S3.

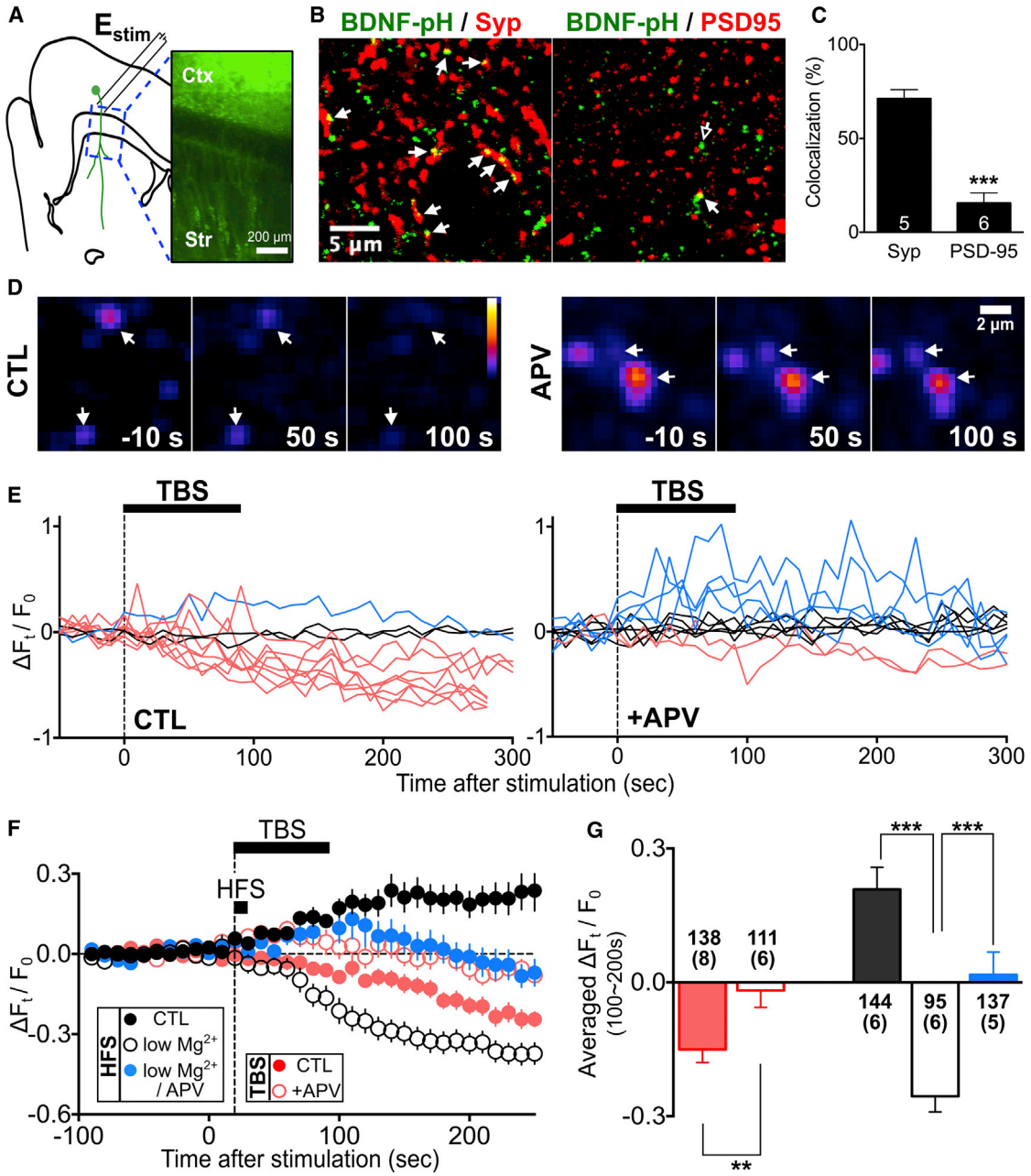

Figure 4. Axonal BDNF-pH Secretion Depends on NMDARs

(A) Left: schematic illustration for imaging activity-induced changes in BDNF-pH fluorescence from cortical axons, using parasagittal corticostriatal slices. E_{stim}, bipolar stimulation electrode placed at layer 6 of M1. Right: fluorescence image of cortical axons expressing BDNF-pH. Ctx, cortex; Str, striatum.

(B) Left: immunostaining images showing colocalization of BDNF-pH puncta with the presynaptic marker synaptophysin (arrowheads), suggesting the presence of BDNF-pH in presynaptic terminals. Right: immunostaining images showing juxtaposition of many BDNF-pH puncta with the postsynaptic marker PSD-95 (empty arrow) but very few colocalized BDNF-pH and PSD-95 puncta (yellow, arrowheads).

(C) Quantitative measurements of colocalization of BDNF-pHluorin puncta with synaptophysin and PSD-95 puncta, normalized by the total BDNF-pH puncta in each optical section (mean ± SEM; ***$p < 0.001$, unpaired t test). Numbers of striatal slices (from 2 mice, one randomly sampled optical section per slice) counted are indicated in the bar.

(D) Example images showing changes in BDNF-pH puncta (arrowheads) fluorescence 10 s before and 50 s and 100 s after TBS in normal recording solution ("CTL") or solution containing APV ("APV").

(E) Sample traces of BDNF-pH puncta fluorescence before and after TBS in CTL (left) and APV (right) conditions. Red, puncta showing fluorescence decreases to a level below the baseline ("fusion with secretion"); blue, fluorescence increases above the baseline ("fusion without secretion"); black, no fluorescence change ("no fusion") after TBS.

(legend continued on next page)

burst (Figure S2). The composite EPSPs triggered by the light burst in postsynaptic MSNs were comparable to those triggered by electrical TBS (Figure S2). Our finding that optical TBS-induced LTP has the same dependence on NMDAR activation and extracellular BDNF as that found for LTP induced by electrical TBS (Figures 1H and 2F) supports the notion that these two types of LTP share common cellular mechanisms. Furthermore, our study demonstrated that, due to the specificity in the axons stimulated, optogenetic LTP is best suited for studying activity-dependent homosynaptic plasticity and the role of presynaptic mechanisms involved, by combining ChR2 expression with genetic manipulation of target genes.

Our data showed that the time course of LTP expression by optogenetic TBS was slower than that of LTP induced by electrical stimulation (compare Figures 1G and 2E; see also Hawes et al., 2013). This may be caused by occasional failures of light-triggered presynaptic spiking in the high-frequency burst (Figure S2), leading to lower synaptic activation during TBS. Other factors, e.g., differences in slice preparation (parasagittal versus coronal) and methods for recording EPSPs (whole-cell current-clamp versus extracellular field recording) may also contribute to difference in rate of LTP induction. Since electrical TBS in parasagittal slices could activate axons originated from diverse cortical areas, whereas optogenetic TBS in coronal slices only stimulated M1 cortical axons expressing ChR2, it is also possible that the electrical versus optical TBS had stimulated different subpopulations of cortical axons that have different MSN target neurons or distinct axon-type-specific time course of LTP induction. This idea is also consistent with the heterogeneity in the efficacy of LTP induction (Partridge et al., 2000) and differential cortical origins of projections in different dorsal striatum subregions (Cospito and Kultas-Ilinsky, 1981; McGeorge and Faull, 1987). Finally, through specific stimulation of M1 cortical axons, our optogenetic TBS may have revealed a specific form of presynaptic BDNF-dependent LTP that is expressed through both pre- and postsynaptic modifications with a slower time course.

Functions of Presynaptic NMDARs in Synaptic Plasticity

The physiological significance of presynaptic NMDARs has been addressed in a few previous studies. Besides the effects of presynaptic NMDAs on autoregulation of glutamate release at hippocampal and cortical synapses (Duguid and Sjöström, 2006; Kunz et al., 2013; McGuinness et al., 2010), there is increasing evidence for the involvement of presynaptic NMDARs in activity-dependent synaptic plasticity. In the lateral amygdala, glutamate released from thalamic inputs may activate presynaptic NMDARs of coactive cortical afferents, resulting in heterosynaptic LTP of cortico-amygdala synapses (Humeau et al., 2003). There is no report so far on the involvement of presynaptic NMDARs in homosynaptic LTP. Presynaptic NMDAR signaling also regulates LTD at cerebellar parallel fiber synapses on Purkinje cells (Casado et al., 2002; Shin and Linden, 2005) and heterosynaptic LTD at GABAergic synapses associated with retinotectal LTP in developing *Xenopus* tectum (Lien et al., 2006). Moreover, coincident activation of presynaptic NMDARs and endocannabinoid receptors was required for spike timing-dependent LTD of synapses between layer 5 pyramidal neurons (Sjöström et al., 2003).

Unlike heterosynaptic LTP of cortical inputs to the lateral amygdala, which is independent of postsynaptic NMDAR activation, LTP of corticostriatal synapses requires the activation of both pre- and postsynaptic NMDARs. Previous studies on striatal slices from striatum-specific *Grin1* knockout mice showed that HFS-induced corticostriatal LTP (observed in low-Mg^{2+} solution) was abolished (Dang et al., 2006), indicating a requirement of NMDARs in postsynaptic MSNs for corticostriatal LTP as confirmed by our result (Figure S2). In addition, we found the actions of axonal NMDARs (Figure 2) on both Ca^{2+} elevation and presynaptic BDNF secretion (Figures 3 and 5). Because secreted BDNF could further exert both pre- and postsynaptic modifications through TrkB receptor-mediated signaling (Poo, 2001), BDNF released from presynaptic axons could be responsible for the expression of potentiated properties on both sides of the synapse.

Physiological Significance of TBS

Neuronal spiking triggered by TBS is known to mimic physiological activities in vivo. For example, theta-frequency activity in dorsal striatal neurons was associated with striatal learning (DeCoteau et al., 2007; Tort et al., 2008), and activation of cortical afferents with the theta-ranged frequency (5 Hz) can induce in vivo corticostriatal LTP without additional manipulation of striatal MSNs (Charpier et al., 1999). Human studies also showed that cortical activation with a theta-burst pattern could enhance the excitability of human motor cortex (Huang et al., 2005) through BDNF-dependent signaling (Cheeran et al., 2008).

In the present study, we found that robust LTP could be induced by TBS under physiological conditions, but not by HFS unless extracellular Mg^{2+} is reduced to a nonphysiological level, although HFS-induced LTP in the normal Mg^{2+} condition has been reported for certain development periods or in specific striatal subregions (Partridge et al., 2000). Pairing presynaptic stimulation with postsynaptic depolarization (Pawlak and Kerr, 2008; Shen et al., 2008) was also effective in NMDAR- and D1/D5R-dependent LTP at corticostriatal synapses, but the same pairing stimulation could also result in LTD induction (Shindou et al., 2011). On the other hand, TBS could reliably induce LTP that requires the activation of both NMDARs and BDNF signaling at both corticostriatal synapses (Figures 1G and 3B; Hawes et al., 2013) and hippocampal synapses (McGuinness et al., 2010; Zakharenko et al., 2001, 2003).

Our results further suggest the distinct effectiveness of TBS in activating presynaptic NMDAR-dependent mechanisms for

(F) Summary of the average fractional fluorescence changes with time ($\Delta F_t/F_0$) for all puncta recorded, as those shown in (E). Mean ± SEM.
(G) Bar graphs depict average $\Delta F_t/F_0$ (±SEM) during 100–200 s after HFS or TBS application for all recorded BDNF-pH puncta. Numbers of puncta and slices (with bracket) are shown with the bars. In TBS: CTL, −0.15 ± 0.03; +APV, −0.018 ± 0.04; **$p < 0.01$, unpaired t test. In HFS: CTL, 0.21 ± 0.05; low Mg^{2+}, −0.26 ± 0.04; low Mg^{2+}/APV, 0.02 ± 0.06; ***$p < 0.001$, one-way ANOVA with post hoc test. See also Figure S4.

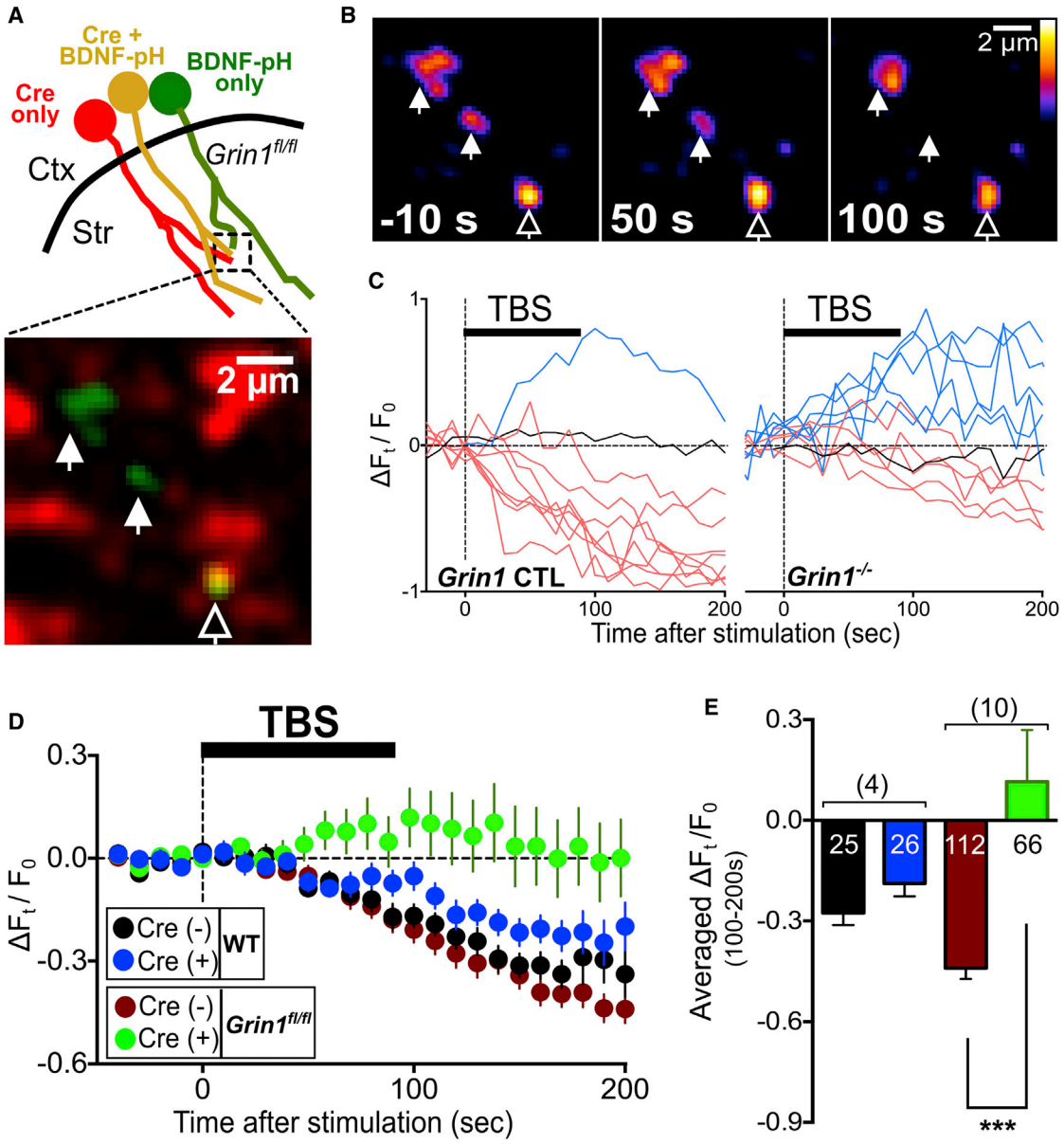

Figure 5. TBS-Induced BDNF Secretion Depends on Functional Axonal NMDARs

(A) Top: schematic diagram shows striatal slices of *Grin1*$^{fl/fl}$ mice expressing either Cre-2a-mCherry (red) or BDNF-pH (green) alone, or both (yellow) in M1 axons. Bottom: fluorescence image showing a dorsal striatal area containing puncta of the above three axon types. Filled arrowheads: axons expressing only BDNF-pH. Empty arrowhead: an axon coexpressing BDNF-pH and Cre.

(B) Fluorescence images of the example puncta in (A) at 10 s before and 50 and 100 s after the onset of TBS. Arrowheads are same as in (A).

(C) Sample traces of BDNF-pH puncta fluorescence before and after TBS, recorded from axons expressing BDNF-pH only (*Grin1* CTL) and coexpressing BDNF-pH and Cre (*Grin1*$^{-/-}$), respectively. Color codes are the same as in Figure 4E.

(D) Average fractional fluorescence changes with time ($\Delta F_t/F_0$) for BDNF-pH puncta of Cre (−) or Cre (+) axons in wild-type WT or *Grin1*$^{fl/fl}$ mice. Mean ± SEM.

(E) Bar graphs represent average $\Delta F_t/F_0$ (±SEM) during 100–200 s after HFS or TBS application for all recorded BDNF-pH puncta. Numbers of puncta and slices (with bracket) are shown with the bars. In WT: Cre (−), −0.28 ± 0.04; Cre (+), −0.19 ± 0.04. In *Grin1*$^{fl/fl}$: Cre (−), −0.28 ± 0.04; Cre (+), 0.02 ± 0.11; ***$p < 0.0001$, unpaired t test. See also Figure S5.

triggering corticostriatal LTP, as compared to HFS. Unlike HFS, TBS was able to induce prolonged axonal Ca^{2+} elevation and presynaptic BDNF secretion under normal Mg^{2+} condition. On the other hand, in the low-Mg^{2+} condition, HFS became highly effective in inducing both NMDAR-dependent axonal Ca^{2+} elevation and BDNF secretion to a level comparable to those induced by TBS (Figures 3 and 4). Finally, LTP induced by both HFS in low Mg^{2+} (Jia et al., 2010) and TBS was fully dependent on extracellular secreted BDNF (Figures 1 and 2), which originated from presynaptic axons.

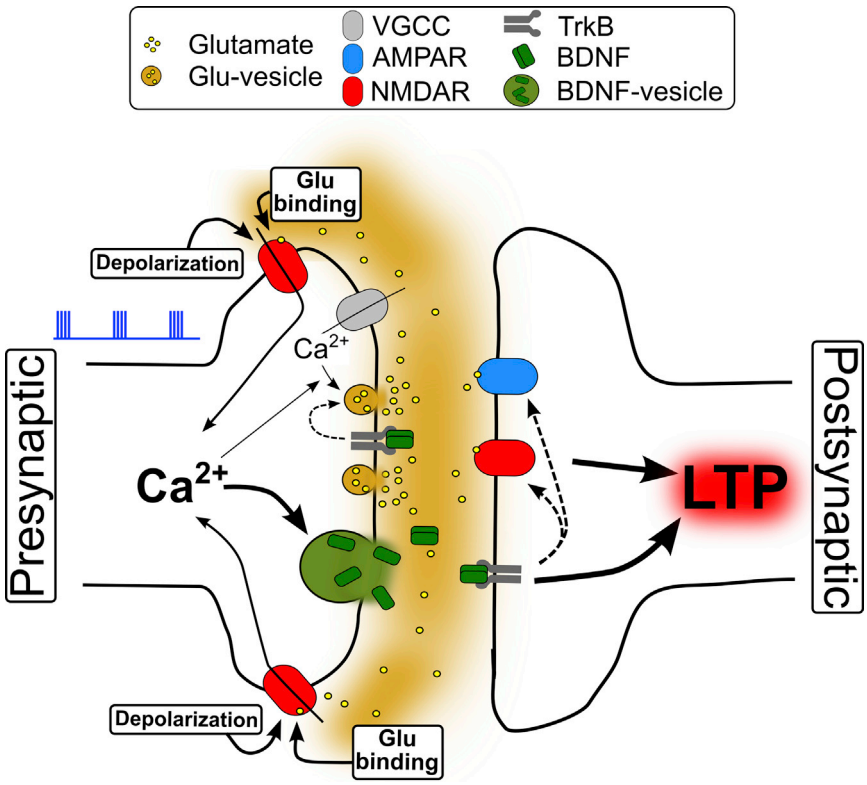

Figure 6. Proposed Model for Presynaptic NMDAR-Regulated BDNF Secretion and LTP Induction

A schematic illustration of presynaptic NMDAR-dependent BDNF secretion from presynaptic axon terminals in response to TBS. We propose that the temporal coincidence in the presence of extracellular glutamate and presynaptic axon depolarization during TBS allows effective activation of presynaptic NMDARs, causing global axonal Ca^{2+} elevation and downstream signaling that induces exocytosis of BDNF-containing granules, a process essential for the induction of corticostriatal LTP.

What mechanisms underlie the effective activation of presynaptic NMDARs by TBS as compared to HFS? Synaptic NMDAR activation requires coincident detection of glutamate binding to the NMDAR subunit and depolarization-induced removal of the Mg^{2+} that blocks the NMDAR channel (Jahr and Stevens, 1987; Mayer et al., 1984). Because increased extracellular glutamate triggered by LTP-inducing stimuli could persist for up to several minutes, as indicated by the slow decay of synaptic activity-evoked glutamate transporter currents in nearby glial cells (Diamond et al., 1998; Lüscher et al., 1998), this increased extracellular glutamate may be responsible for activation of presynaptic NMDARs. Although the amounts of released glutamate TBS versus HFS (with the same number of spikes) are unlikely to be substantially different, temporal spreading of spikes in the TBS pattern provides a more extended coincident action of extracellular glutamate on presynaptic NMDARs due to a much longer period of axonal membrane depolarization than HFS. This idea is supported by the findings that axonal firing at theta frequency is more efficient for enhancing transmitter release via presynaptic NMDARs as compared to other stimulation frequencies (McGuinness et al., 2010), and HFS induced only a low-level global Ca^{2+} increase unless low-Mg^{2+} solution was used (Figure 3C).

Mechanisms Regulating BDNF Secretion

We demonstrated an axonal NMDAR-dependent BDNF secretion by two-photon imaging of cortical axons expressing BDNF-pH in corticostriatal slices. Previous studies using the same BDNF-pH expression in cultured hippocampal neurons showed that substantial pro-BDNF-pH was found in cell lysates but not in the extracellular medium, indicating that secreted BDNF-pH is mostly in the mature form (Matsuda et al., 2009). This is consistent with the previous finding on the secretion of BDNF protein fused with other fluorescent proteins (Haubensak et al., 1998). The extent of TrkB phosphorylation induced by secreted BDNF-pH in cultured cortical neurons was also similar to that induced by recombinant human BDNF (Matsuda et al., 2009). Thus, BDNF-pH is biologically active and could serve as a good tracer for studying the dynamics of endogenous BDNF secretion.

Although activity-induced BDNF secretion from cultured neurons depends on NMDAR activities (Lever et al., 2001; Marini et al., 1998; Matsuda et al., 2009), it has been unclear whether this involves axonal or dendritic NMDARs, or both. We now provide direct evidence that axonal NMDARs are responsible for triggering presynaptic BDNF secretion by mediating prolonged Ca^{2+} elevation. The requirement of cytoplasmic Ca^{2+} elevation and corresponding Ca^{2+} sensors are likely to be different for exocytosis of synaptic vesicles versus secretory granules (Lessmann and Brigadski, 2009; Pang and Südhof, 2010). We found that HFS (in normal Mg^{2+} solution) triggered only a low-level Ca^{2+} accumulation in the axon terminals and caused fusion pore formation of the BDNF-containing granules without exocytic BDNF secretion, whereas NMDAR-mediated prolonged Ca^{2+} elevation (caused by either TBS in normal-Mg^{2+}or HFS in low-Mg^{2+} solution) produced full exocytic BDNF secretion (Figures 4 and 5). In contrast to the dependence of synaptic vesicle exocytosis on high-level transient Ca^{2+} elevation within microdomains around voltage-dependent Ca^{2+} channels (Neher, 1998), NMDAR-mediated large Ca^{2+} influx and Ca^{2+} release from internal stores (Figure 3) appear to regulate exocytosis of BDNF-containing secretory granules via downstream signaling cascades, including specific synaptotagmin isoforms associated with these granules. Indeed, full exocytosis of dense core vesicle in adrenal chromaffin cells requires synaptotagmin 7, which has a higher affinity and slower binding to Ca^{2+} than that of synaptotagmin 1 (Sugita et al., 2002; Schonn et al.,

2008), which regulates synaptic vesicle secretion. Our finding on the role of cortical axonal NMDARs in triggering BDNF secretion and LTP induction at corticostriatal synapses may thus reflect a general function of presynaptic NMDARs in regulating secretory granule exocytosis.

EXPERIMENTAL PROCEDURES

Animals

Animal protocols were approved by the Animal Care and Use Committee of UC Berkeley. All mice were purchased from The Jackson Laboratory. We used 8- to 10-week-old C57BL/6 mice (male) for the wild-type control. For optogenetic LTP recording, GCaMP5, or BDNF-pHluorin imaging, 6- to 8-week-old heterozygous male *CaMKIIa-Cre* (genetic background of C57BL/6; *Tg(Camk2a-cre)T29-1Stl/J*), *Emx1-Cre* (genetic background of C57BL/6; *Emx1tm1(cre)Krj*/J), homozygous *Grin1*$^{fl/fl}$ (genetic background of C57BL/6; *Grin1tm2Stl*/J), or homozygous *Bdnf*$^{fl/fl}$ mice (mixed background of C57BL/6, 129S4/SvJae and BALB/c; *Bdnftm3Jae/J*) were used for AAV injection. Heterozygous *Bdnf-myc* mice (mixed background of C57BL/6 and 129S/Sv) were gift from Dr. Yves Barde.

Electrophysiology

Standard artificial cerebral spinal fluid (ACSF) consisted of 130 mM NaCl, 3.5 mM KCl, 1.25 mM NaH_2PO_4, 24 mM $NaHCO_3$, 2 mM $CaCl_2$, 2 mM $MgCl_2$, and 10 mM glucose (pH 7.3). Mice were deeply anesthetized with isoflurane and then transcardially perfused with ~20 ml of slicing ACSF (ACSF containing 10 mM Mg^{2+} and 0.5 mM Ca^{2+}) before the brain was dissected. Parasagittal striatal slices (400 μm thick) were prepared using a vibratome (Leica) using ice-cold slicing ACSF (below 4°C) and maintained at 30°C–32°C in normal ACSF for 1 hr before electrophysiological recording or two-photon imaging. Slices were placed in a recording chamber, submerged, and continuously perfused (2–3 ml/min) with oxygenated ACSF (containing 100 μM picrotoxin to isolate the glutamatergic synaptic transmission) at room temperature (20°C–25°C).

Whole-cell current-clamp recording was made with a Multiclamp 700B amplifier (Molecular Devices). Data were filtered at 2 kHz, digitized at 1–5 kHz, stored on a computer, and analyzed offline using pCLAMP 10 (Axon Instruments). Striatal MSNs were visualized with infrared differential interference optics equipped with a 40× water-immersion objective and identified by the following intrinsic membrane properties: resting membrane potential more negative than −80 mV, inward rectification in response to somatic current injection, and a long depolarizing ramp prior to spiking. Borosilicate glass patch electrodes had a resistance of 3–5 MΩ after filling with the pipette solution that contains 140 mM K-gluconate, 5 mM KCl, 0.2 mM EGTA, 2 mM $MgCl_2$, 4 mM Mg-ATP, 0.3 mM Na_2-GTP, 10 mM Na_2-phosphocreatine, and 10 mM HEPES (pH 7.3, 290–300 mOsm) for whole-cell current-clamp recording of EPSP.

For LTP experiments using electrical stimulation, a tungsten bipolar electrode (WPI) was placed on the cortical layer 6 close to the white matter, and test stimuli were applied at 0.5 Hz to examine EPSP. Recordings were rejected if V_m changed by more than 10%, input resistance changed by more than 30% during recordings, or the peak amplitude of baseline EPSP was less than 2 mV. After 10 min of recording stable responses, HFS (4 trains of stimuli spaced at 10 s intervals, with each train containing bursts of 100 spikes at 100 Hz) or TBS (10 trains of stimuli spaced at 10 s intervals, with each train containing bursts of 4 spikes at 100 Hz and repeated 10 times at 5 Hz) was delivered. The data for EPSP amplitudes were presented as averages over 1 min bins. For optogenetic induction of corticostriatal LTP, an AAV containing Cre-dependent $ChETA_{TC}$ expression cassette (AAV-EF1a-DIO-hChR2(E123T/T159C)-EYFP; UNC Vector Core) was coinjected with AAV-CMV-Cre-2A-mCherry (Vector Biolabs) with 1:1 genome copy (GC) ratio (0.5 μl in each hemisphere at a titer of ~1 × 10^{12} GC per μl) into M1 of C57BL/6 wild-type, *Grin1*$^{fl/fl}$, or *Bdnf*$^{fl/fl}$ mice using the following stereotaxic coordinates: AP = + 0.2, ML = ± 0.17, DV = −0.10 (in mm). At least 4 weeks were allowed for full expression of $ChETA_{TC}$ and Cre (mCherry). Preparation of coronal striatal slices (400 μm) and whole-cell recording from MSN cells were performed as described above. High-power blue LED (at 490 nm) with a collimator (Thorlabs) was mounted on a microscope (Nikon) and delivered to the slice by a LED driver (Thorlabs). Using 40× objective lens, this configuration could deliver blue light at ~8 mW/mm^2 over ~0.20 mm^2 area of recording slices. With 0.2–1 ms durations of LED illumination, these conditions were sufficient for eliciting stable EPSPs ranging from 1.0 to 10 mV.

Expression of BDNF-pH and GCaMP5

AAV-DIO-BDNF-pHluorin was constructed by inserting BDNF-pHluorin fragment into AAV-DIO vector. For making a custom AAV-DIO vector, double-floxed (floxed with two loxPs and lox2722s) gene insertion cassette from pJ241-Flex (Addgene plasmid 18925) was inserted into AAV-EF1a vector through KpnI and EcoRI restriction enzyme sites. Then, PCR-amplified BDNF-pHluorin from pCMV5b-BDNF-pHluorin was inserted into AAV-DIO vector through SpeI restriction enzyme site to construct AAV-DIO-BDNF-pHluroin. Sequencing and restriction enzyme reactions were performed to verify the plasmid. For making AAV-hSyn-BDNF-pHluorin, AAV-hSyn-ChR2-EYFP was digested with KpnI and EcoRV restriction enzymes to produce AAV-hSyn vector. PCR amplified BDNF-pHluorin was inserted with same enzyme sites. Packaging (serotype 5) and purification of AAV-DIO-BDNF-pHluorin were carried out by UNC Vector Core. AAV-hSyn-BDNF-pHluorin was packaged (serotype 2) and purified as reported previously (Maheshri et al., 2006). AAV-Flex-GCaMP5 and AAV-hSyn-GCaMP5 were purchased from Penn Vector Core.

AAV-DIO-BDNF-pHluorin or AAV-Flex-GCaMP5 was injected into the M1 of *Emx1-Cre* mice (500 nl per each hemisphere). For conditional GluN1 knockout, AAV-CMV-Cre-2A-mCherry mixed with AAV-hSyn-BDNF-pH or AAV-hSyn-GCaMP5 (1:2 ratio of GC ratio; total 500 nl per hemisphere) was injected into the M1 of *Grin1*$^{fl/fl}$ mice.

Two-Photon Laser-Scanning Microscopy

Two-photon laser-scanning microscopy was performed using an LSM 510 META/NLO Axioimager system (Zeiss; Molecular Imaging Center at UC Berkeley) equipped with a Spectra-Physics MaiTai HP DeepSee laser (700 to 1,020 nm) and 40× water-immersion infrared objective (NA 0.8). BDNF-pH and GCaMP5 were excited by the 880 nm laser. The emission signals of BDNF-pH and GCaMP5 were acquired using 500–550 nm band-pass filter. The filed of view (512 × 512 pixels, 0.21 μm/pixel, 0.8 μs pixel time) was chosen in the striatal slice where cortical projections remained intact and BDNF-pH or GCaMP5 were significantly expressed at synaptic bouton-like structure (1–2 μm).

To record changes in BDNF-pH or GCaMP5 intensity in response to electrical stimulation, we acquired at least 100 consecutive images (at 1 Hz) as a baseline, applied electrical stimulation using a tungsten bipolar electrode (WPI) placed on the cortical layer 6 close to the white matter, and then at least additional 200 images at 1 Hz after stimulation were taken. To perform dual channel imaging for BDNF-pH or GCaMP5 and mCherry, we used single 780 or 880 nm laser light for excitation but emissions were independently acquired using different emission filters (500–530 nm band-pass filter for BDNF-pH and 560 nm long-pass filter for mCherry). In some experiments, iso-osmotic ACSF containing 50 mM NH_4Cl (pH 7.4) was applied to identify axonal BDNF-pH at the end of each experiment.

Statistical Analysis

Statistical analyses were performed by using Prism 6.0 software (Graphpad). Kolmogorov-Smirnov test was used for testing significance of cumulative percentage plot of mean EPSP amplitudes. Unpaired Student's t test and one-way ANOVA with post hoc test were used for testing significance between two groups and among three or more groups, respectively.

SUPPLEMENTAL INFORMATION

Supplemental Information includes Supplemental Experimental Procedures and five figures and can be found with this article online at http://dx.doi.org/10.1016/j.neuron.2014.10.045.

ACKNOWLEDGMENTS

We thank Dr. Karl Deisseroth for the gift of AAV-hSyn-ChR2-EYFP and AAV-DIO-ChETA$_{TC}$-EYFP constructs, Dr. Yves Barde for BDNF-MYC mice, and Dr. Seung Hee Lee for assistance in preparing AAV-hSyn-BDNF-pHluorin. This work was supported by grants from the US National Institutes of Health (NIH NS 036999) and the CHDI foundation (CHDI A3794).

Accepted: October 16, 2014
Published: November 20, 2014

REFERENCES

Akerboom, J., Chen, T.W., Wardill, T.J., Tian, L., Marvin, J.S., Mutlu, S., Calderón, N.C., Esposti, F., Borghuis, B.G., Sun, X.R., et al. (2012). Optimization of a GCaMP calcium indicator for neural activity imaging. J. Neurosci. *32*, 13819–13840.

Altar, C.A., Cai, N., Bliven, T., Juhasz, M., Conner, J.M., Acheson, A.L., Lindsay, R.M., and Wiegand, S.J. (1997). Anterograde transport of brain-derived neurotrophic factor and its role in the brain. Nature *389*, 856–860.

Bear, M.F., and Malenka, R.C. (1994). Synaptic plasticity: LTP and LTD. Curr. Opin. Neurobiol. *4*, 389–399.

Berndt, A., Schoenenberger, P., Mattis, J., Tye, K.M., Deisseroth, K., Hegemann, P., and Oertner, T.G. (2011). High-efficiency channelrhodopsins for fast neuronal stimulation at low light levels. Proc. Natl. Acad. Sci. USA *108*, 7595–7600.

Brasier, D.J., and Feldman, D.E. (2008). Synapse-specific expression of functional presynaptic NMDA receptors in rat somatosensory cortex. J. Neurosci. *28*, 2199–2211.

Calabresi, P., Pisani, A., Mercuri, N.B., and Bernardi, G. (1992). Long-term potentiation in the striatum is unmasked by removing the voltage-dependent magnesium block of NMDA receptor channels. Eur. J. Neurosci. *4*, 929–935.

Casado, M., Isope, P., and Ascher, P. (2002). Involvement of presynaptic N-methyl-D-aspartate receptors in cerebellar long-term depression. Neuron *33*, 123–130.

Charpier, S., Mahon, S., and Deniau, J.M. (1999). In vivo induction of striatal long-term potentiation by low-frequency stimulation of the cerebral cortex. Neuroscience *91*, 1209–1222.

Cheeran, B., Talelli, P., Mori, F., Koch, G., Suppa, A., Edwards, M., Houlden, H., Bhatia, K., Greenwood, R., and Rothwell, J.C. (2008). A common polymorphism in the brain-derived neurotrophic factor gene (BDNF) modulates human cortical plasticity and the response to rTMS. J. Physiol. *586*, 5717–5725.

Conner, J.M., Lauterborn, J.C., Yan, Q., Gall, C.M., and Varon, S. (1997). Distribution of brain-derived neurotrophic factor (BDNF) protein and mRNA in the normal adult rat CNS: evidence for anterograde axonal transport. J. Neurosci. *17*, 2295–2313.

Cospito, J.A., and Kultas-Ilinsky, K. (1981). Synaptic organization of motor corticostriatal projections in the rat. Exp. Neurol. *72*, 257–266.

Dang, M.T., Yokoi, F., Yin, H.H., Lovinger, D.M., Wang, Y., and Li, Y. (2006). Disrupted motor learning and long-term synaptic plasticity in mice lacking NMDAR1 in the striatum. Proc. Natl. Acad. Sci. USA *103*, 15254–15259.

DeCoteau, W.E., Thorn, C., Gibson, D.J., Courtemanche, R., Mitra, P., Kubota, Y., and Graybiel, A.M. (2007). Learning-related coordination of striatal and hippocampal theta rhythms during acquisition of a procedural maze task. Proc. Natl. Acad. Sci. USA *104*, 5644–5649.

Diamond, J.S., Bergles, D.E., and Jahr, C.E. (1998). Glutamate release monitored with astrocyte transporter currents during LTP. Neuron *21*, 425–433.

Dieni, S., Matsumoto, T., Dekkers, M., Rauskolb, S., Ionescu, M.S., Deogracias, R., Gundelfinger, E.D., Kojima, M., Nestel, S., Frotscher, M., and Barde, Y.-A. (2012). BDNF and its pro-peptide are stored in presynaptic dense core vesicles in brain neurons. J. Cell Biol. *196*, 775–788.

Duguid, I., and Sjöström, P.J. (2006). Novel presynaptic mechanisms for coincidence detection in synaptic plasticity. Curr. Opin. Neurobiol. *16*, 312–322.

Faber, D.S., and Korn, H. (1991). Applicability of the coefficient of variation method for analyzing synaptic plasticity. Biophys. J. *60*, 1288–1294.

Figurov, A., Pozzo-Miller, L.D., Olafsson, P., Wang, T., and Lu, B. (1996). Regulation of synaptic responses to high-frequency stimulation and LTP by neurotrophins in the hippocampus. Nature *381*, 706–709.

Hartmann, M., Heumann, R., and Lessmann, V. (2001). Synaptic secretion of BDNF after high-frequency stimulation of glutamatergic synapses. EMBO J. *20*, 5887–5897.

Haubensak, W., Narz, F., Heumann, R., and Lessmann, V. (1998). BDNF-GFP containing secretory granules are localized in the vicinity of synaptic junctions of cultured cortical neurons. J. Cell Sci. *111*, 1483–1493.

Hawes, S.L., Gillani, F., Evans, R.C., Benkert, E.A., and Blackwell, K.T. (2013). Sensitivity to theta-burst timing permits LTP in dorsal striatal adult brain slice. J. Neurophysiol. *110*, 2027–2036.

Huang, Y.Z., Edwards, M.J., Rounis, E., Bhatia, K.P., and Rothwell, J.C. (2005). Theta burst stimulation of the human motor cortex. Neuron *45*, 201–206.

Humeau, Y., Shaban, H., Bissière, S., and Lüthi, A. (2003). Presynaptic induction of heterosynaptic associative plasticity in the mammalian brain. Nature *426*, 841–845.

Jahr, C.E., and Stevens, C.F. (1987). Glutamate activates multiple single channel conductances in hippocampal neurons. Nature *325*, 522–525.

Jia, Y., Gall, C.M., and Lynch, G. (2010). Presynaptic BDNF promotes postsynaptic long-term potentiation in the dorsal striatum. J. Neurosci. *30*, 14440–14445.

Korte, M., Carroll, P., Wolf, E., Brem, G., Thoenen, H., and Bonhoeffer, T. (1995). Hippocampal long-term potentiation is impaired in mice lacking brain-derived neurotrophic factor. Proc. Natl. Acad. Sci. USA *92*, 8856–8860.

Kunz, P.A., Roberts, A.C., and Philpot, B.D. (2013). Presynaptic NMDA receptor mechanisms for enhancing spontaneous neurotransmitter release. J. Neurosci. *33*, 7762–7769.

Larsen, R.S., Corlew, R.J., Henson, M.A., Roberts, A.C., Mishina, M., Watanabe, M., Lipton, S.A., Nakanishi, N., Pérez-Otaño, I., Weinberg, R.J., and Philpot, B.D. (2011). NR3A-containing NMDARs promote neurotransmitter release and spike timing-dependent plasticity. Nat. Neurosci. *14*, 338–344.

Lessmann, V., and Brigadski, T. (2009). Mechanisms, locations, and kinetics of synaptic BDNF secretion: an update. Neurosci. Res. *65*, 11–22.

Lever, I.J., Bradbury, E.J., Cunningham, J.R., Adelson, D.W., Jones, M.G., McMahon, S.B., Marvizón, J.C., and Malcangio, M. (2001). Brain-derived neurotrophic factor is released in the dorsal horn by distinctive patterns of afferent fiber stimulation. J. Neurosci. *21*, 4469–4477.

Lien, C.C., Mu, Y., Vargas-Caballero, M., and Poo, M.M. (2006). Visual stimuli-induced LTD of GABAergic synapses mediated by presynaptic NMDA receptors. Nat. Neurosci. *9*, 372–380.

Lovinger, D.M. (2010). Neurotransmitter roles in synaptic modulation, plasticity and learning in the dorsal striatum. Neuropharmacology *58*, 951–961.

Lüscher, C., Malenka, R.C., and Nicoll, R.A. (1998). Monitoring glutamate release during LTP with glial transporter currents. Neuron *21*, 435–441.

Maheshri, N., Koerber, J.T., Kaspar, B.K., and Schaffer, D.V. (2006). Directed evolution of adeno-associated virus yields enhanced gene delivery vectors. Nat. Biotechnol. *24*, 198–204.

Marini, A.M., Rabin, S.J., Lipsky, R.H., and Mocchetti, I. (1998). Activity-dependent release of brain-derived neurotrophic factor underlies the neuroprotective effect of N-methyl-D-aspartate. J. Biol. Chem. *273*, 29394–29399.

Matsuda, N., Lu, H., Fukata, Y., Noritake, J., Gao, H., Mukherjee, S., Nemoto, T., Fukata, M., and Poo, M.M. (2009). Differential activity-dependent secretion of brain-derived neurotrophic factor from axon and dendrite. J. Neurosci. *29*, 14185–14198.

Matsumoto, T., Rauskolb, S., Polack, M., Klose, J., Kolbeck, R., Korte, M., and Barde, Y.-A. (2008). Biosynthesis and processing of endogenous BDNF: CNS neurons store and secrete BDNF, not pro-BDNF. Nat. Neurosci. *11*, 131–133.

Mayer, M.L., Westbrook, G.L., and Guthrie, P.B. (1984). Voltage-dependent block by Mg2+ of NMDA responses in spinal cord neurones. Nature *309*, 261–263.

McGeorge, A.J., and Faull, R.L. (1987). The organization and collateralization of corticostriate neurones in the motor and sensory cortex of the rat brain. Brain Res. *423*, 318–324.

McGuinness, L., Taylor, C., Taylor, R.D.T., Yau, C., Langenhan, T., Hart, M.L., Christian, H., Tynan, P.W., Donnelly, P., and Emptage, N.J. (2010). Presynaptic NMDARs in the hippocampus facilitate transmitter release at theta frequency. Neuron *68*, 1109–1127.

Neher, E. (1998). Vesicle pools and Ca2+ microdomains: new tools for understanding their roles in neurotransmitter release. Neuron *20*, 389–399.

Pang, Z.P., and Südhof, T.C. (2010). Cell biology of Ca2+-triggered exocytosis. Curr. Opin. Cell Biol. *22*, 496–505.

Park, H., and Poo, M.M. (2013). Neurotrophin regulation of neural circuit development and function. Nat. Rev. Neurosci. *14*, 7–23.

Partridge, J.G., Tang, K.C., and Lovinger, D.M. (2000). Regional and postnatal heterogeneity of activity-dependent long-term changes in synaptic efficacy in the dorsal striatum. J. Neurophysiol. *84*, 1422–1429.

Patterson, S.L.S., Abel, T., Deuel, T.A.T., Martin, K.C.K., Rose, J.C.J., and Kandel, E.R.E. (1996). Recombinant BDNF rescues deficits in basal synaptic transmission and hippocampal LTP in BDNF knockout mice. Neuron *16*, 1137–1145.

Pawlak, V., and Kerr, J.N. (2008). Dopamine receptor activation is required for corticostriatal spike-timing-dependent plasticity. J. Neurosci. *28*, 2435–2446.

Peng, Y.Y., and Zucker, R.S. (1993). Release of LHRH is linearly related to the time integral of presynaptic Ca2+ elevation above a threshold level in bullfrog sympathetic ganglia. Neuron *10*, 465–473.

Pennartz, C.M.A., Berke, J.D., Graybiel, A.M., Ito, R., Lansink, C.S., van der Meer, M., Redish, A.D., Smith, K.S., and Voorn, P. (2009). Corticostriatal Interactions during Learning, Memory Processing, and Decision Making. J. Neurosci. *29*, 12831–12838.

Poo, M.M. (2001). Neurotrophins as synaptic modulators. Nat. Rev. Neurosci. *2*, 24–32.

Pozzo-Miller, L.D., Gottschalk, W., Zhang, L., McDermott, K., Du, J., Gopalakrishnan, R., Oho, C., Sheng, Z.H., and Lu, B. (1999). Impairments in high-frequency transmission, synaptic vesicle docking, and synaptic protein distribution in the hippocampus of BDNF knockout mice. J. Neurosci. *19*, 4972–4983.

Schonn, J.S., Maximov, A., Lao, Y., Südhof, T.C., and Sørensen, J.B. (2008). Synaptotagmin-1 and -7 are functionally overlapping Ca2+ sensors for exocytosis in adrenal chromaffin cells. Proc. Natl. Acad. Sci. USA *105*, 3998–4003.

Shen, W., Flajolet, M., Greengard, P., and Surmeier, D.J. (2008). Dichotomous dopaminergic control of striatal synaptic plasticity. Science *321*, 848–851.

Shin, J.H., and Linden, D.J. (2005). An NMDA receptor/nitric oxide cascade is involved in cerebellar LTD but is not localized to the parallel fiber terminal. J. Neurophysiol. *94*, 4281–4289.

Shindou, T., Ochi-Shindou, M., and Wickens, J.R. (2011). A Ca(2+) threshold for induction of spike-timing-dependent depression in the mouse striatum. J. Neurosci. *31*, 13015–13022.

Sjöström, P.J., Turrigiano, G.G., and Nelson, S.B. (2003). Neocortical LTD via coincident activation of presynaptic NMDA and cannabinoid receptors. Neuron *39*, 641–654.

Sugita, S., Shin, O.H., Han, W., Lao, Y., and Südhof, T.C. (2002). Synaptotagmins form a hierarchy of exocytotic Ca(2+) sensors with distinct Ca(2+) affinities. EMBO J. *21*, 270–280.

Tort, A.B., Kramer, M.A., Thorn, C., Gibson, D.J., Kubota, Y., Graybiel, A.M., and Kopell, N.J. (2008). Dynamic cross-frequency couplings of local field potential oscillations in rat striatum and hippocampus during performance of a T-maze task. Proc. Natl. Acad. Sci. USA *105*, 20517–20522.

Tsien, J.Z., Huerta, P.T., and Tonegawa, S. (1996). The essential role of hippocampal CA1 NMDA receptor-dependent synaptic plasticity in spatial memory. Cell *87*, 1327–1338.

Wang, H., and Pickel, V.M. (2000). Presence of NMDA-type glutamate receptors in cingulate corticostriatal terminals and their postsynaptic targets. Synapse *35*, 300–310.

Zakharenko, S.S., Zablow, L., and Siegelbaum, S.A. (2001). Visualization of changes in presynaptic function during long-term synaptic plasticity. Nat. Neurosci. *4*, 711–717.

Zakharenko, S.S., Patterson, S.L., Dragatsis, I., Zeitlin, S.O., Siegelbaum, S.A., Kandel, E.R., and Morozov, A. (2003). Presynaptic BDNF required for a presynaptic but not postsynaptic component of LTP at hippocampal CA1-CA3 synapses. Neuron *39*, 975–990.